Bioactive Materials 19 (2023) 538–549

Contents lists available at ScienceDirect

Bioactive Materials

journal homepage: www.keaipublishing.com/en/journals/bioactive-materials

Polymeric dual-modal imaging nanoprobe with two-photon aggregation-induced emission for fluorescence imaging and gadolinium-chelation for magnetic resonance imaging

Xueyang Xiao [a,1], Hao Cai [a,1], Qiaorong Huang [a], Bing Wang [a], Xiaoming Wang [a], Qiang Luo [a], Yinggang Li [a], Hu Zhang [c], Qiyong Gong [a,b], Xuelei Ma [a,**], Zhongwei Gu [a], Kui Luo [a,b,*]

[a] Department of Radiology, Department of Biotherapy, Huaxi MR Research Center (HMRRC), Laboratory of Stem Cell Biology, Cancer Center, Department of Ultrasound, National Clinical Research Center for Geriatrics, Frontiers Science Center for Disease-Related Molecular Network, State Key Laboratory of Biotherapy, West China Hospital, Sichuan University, Chengdu, 610041, China

[b] Functional and Molecular Imaging Key Laboratory of Sichuan Province, Research Unit of Psychoradiology, Chinese Academy of Medical Sciences, Chengdu, 610041, China

[c] Amgen Bioprocessing Centre, Keck Graduate Institute, CA, 91711, USA

ARTICLE INFO

Keywords:
RAFT polymerization
Amphiphilic block polymers
Magnetic resonance/fluorescence dual-modal imaging
Tumor/vascular imaging
Two-photon AIE fluorescent contrast agent

ABSTRACT

Nanoprobes that offer both fluorescence imaging (FI) and magnetic resonance imaging (MRI) can provide supplementary information and hold synergistic advantages. However, synthesis of such dual-modality imaging probes that simultaneously exhibit tunability of functional groups, high stability, great biocompatibility and desired dual-modality imaging results remains challenging. In this study, we used an amphiphilic block polymer from (ethylene glycol) methyl ether methacrylate (OEGMA) and *N*-(2-hydroxypropyl) methacrylamide (HPMA) derivatives as a carrier to conjugate a MR contrast agent, Gd-DOTA, and a two-photon fluorophore with an aggregation-induced emission (AIE) effect, TPBP, to construct a MR/two-photon fluorescence dual-modality contrast agent, Gd-DOTA-TPBP. Incorporation of gadolinium in the hydrophilic chain segment of the OEGMA-based carrier resulted in a high r_1 value for Gd-DOTA-TPBP, revealing a great MR imaging resolution. The contrast agent specifically accumulated in the tumor region, allowing a long enhancement duration for vascular and tumor contrast-enhanced MR imaging. Meanwhile, coupling TPBP with AIE properties to the hydrophobic chain segment of the carrier not only improved its water solubility and reduced its cytotoxicity, but also significantly enhanced its imaging performance in an aqueous phase. Gd-DOTA-TPBP was also demonstrated to act as an excellent fluorescence probe for two-photon-excited bioimaging with higher resolution and greater sensitivity than MRI. Since high-resolution, complementary MRI/FI dual-modal images were acquired at both cellular and tissue levels in tumor-bearing mice after application of Gd-DOTA-TPBP, it has great potential in the early phase of disease diagnosis.

1. Introduction

Medical imaging is one of the most important tools for clinical diagnosis, monitoring of therapeutic outcomes, and evaluation of prognosis. Different medical imaging modalities have their unique advantages and drawbacks, therefore, two or more combined imaging modalities have received rising attention in recent years [1,2]. Magnetic resonance imaging (MRI) is one of the most widely used imaging methods in clinic [3,4]. It has great spatial resolution and can image a deep tissue structure, but its imaging sensitivity is poor. Fluorescence

Peer review under responsibility of KeAi Communications Co., Ltd.

* Corresponding author. Department of Radiology, Department of Biotherapy, Huaxi MR Research Center (HMRRC), Laboratory of Stem Cell Biology, Cancer Center, Department of Ultrasound, National Clinical Research Center for Geriatrics, Frontiers Science Center for Disease-Related Molecular Network, State Key Laboratory of Biotherapy, West China Hospital, Sichuan University, Chengdu, 610041, China.

** Corresponding author.

E-mail addresses: maxuelei0726@wchscu.cn (X. Ma), luokui@scu.edu.cn (K. Luo).

[1] These authors contributed equally.

https://doi.org/10.1016/j.bioactmat.2022.04.026

Received 28 January 2022; Received in revised form 23 April 2022; Accepted 24 April 2022

imaging (FI) is a popular tool for preclinical experimental research and has been applied in clinic with high imaging sensitivity but a shallow imaging depth [5,6]. Thus, dual-modality imaging that combines MRI and FI would be complementary. The majority of current commercial MRI and FI contrast agents are small molecules, and they have some inherent issues, such as a low relaxivity, a short blood circulation time, a low water solubility, high biological toxicity, and no targeting function [7,8]. Therefore, it is important to develop novel delivery carriers to improve imaging applicability of small molecular contrast agents so that they can be translated for clinical use.

It has been widely reported that polymer-based MRI/FI bimodal contrast agents are able to increase aqueous solubility, reduce biotoxicity, and improve lesion targeting of small-molecular contrast agents, thus they have great potential in MRI and fluorescence imaging [9–12]. However, MRI/FI dual-modality contrast agents need to accommodate differences in physicochemical properties and imaging characteristics between MRI and FI probes through modulating the carrier structure. Due to the structural complexity, it is still challenging to construct bimodal imaging contrast agents with great tunability as well as optimized bimodal imaging results. Recently, due to its ease of use and compatibility with various monomers, reversible addition-fragmentation chain transfer (RAFT) polymerization has become one of the most commonly used methods for controlled preparation of multifunctional polymer carriers [13,14]. Meanwhile, click chemistry has been widely used in the multifunctional modification of polymers due to its mild reaction conditions and extremely high reaction efficiency [15–17]. Therefore, MRI/FI dual-modality contrast agents could be prepared and their properties optimized to achieve the optimal imaging performance of each individual probe through these efficient synthetic methods such as RAFT polymerization and click chemistry.

The MRI contrast agents currently used in clinics are mainly hydrophilic small molecular gadolinium-based chelates. The MR signal enhancement of paramagnetic Gd(III) is principally achieved by increasing the longitudinal relaxation rate of surrounding water protons [18]. Therefore, full contact or coordination between gadolinium contrast agents and water protons is extremely important for polymer-based MRI contrast agents. Besides, according to the Solomon-Bloembergen-Morgan theory [18,19], the rotational correlation time of gadolinium is a key factor for the relaxivity of gadolinium-based contrast agents, and this key factor is strongly influenced by structural characteristics of MRI contrast agents. It has been demonstrated that coupling small-molecular gadolinium-based contrast agents to hydrophilic polymers can increase their rotational correlation time, thereby increasing their relaxivity [20,21]. Different with gadolinium-based contrast agents, the majority of currently used small-molecular fluorescent probes are hydrophobic compounds that have aggregation-caused quenching (ACQ) effects in an aqueous solution, and these effects often impair their imaging performance [22].

Fortunately, with the discovery of the aggregation-induced emission (AIE) effect, many fluorescent molecules with the AIE effect have been reported [23–26]. Due to restriction of intramolecular motions, these AIE molecules display significant fluorescence emission improvement in the aggregated state and have gained great interest in the medical imaging field. In addition, most of traditional fluorescent contrast agents are excited by single photon during imaging, which have drawbacks, for example, a shallow imaging depth and severe optical damage to live tissues or cells. Compared with single-photon excitation, in the two-photon excitation mode, a long wavelength is used for excitation and a short wavelength for emission [27]. This mode has the advantages of a deeper imaging depth, less optical damage and lower background signal, which is more conducive to *in vivo* medical imaging. A few two-photon fluorescent probes with the AIE effect have been reported. For example, Ma et al. reported a two-photon (TP) fluorophore with the AIE property based on triphenylamine structure and pyridinium group [28]. Compared with traditional two-photon fluorescent dyes, this probe allows chemical modification, achieves a deep tissue penetration depth and a high imaging resolution, and demonstrates promising application prospects in two-photon fluorescence imaging. Therefore, based on imaging characteristics of gadolinium and the fluorescent probe with the AIE effect, amphiphilic block polymers could be employed as a carrier to load both MRI and AIE fluorescent probes onto hydrophilic and hydrophobic chain segments of block polymers, respectively, thus MRI/FI dual-modality imaging contrast agents could be obtained to achieve optimal imaging results for both probes. To our knowledge, the design and preparation of polymer-based MRI/TP AIE FI dual-modality contrast agents in consideration of the carrier structure and the imaging properties of different probes has been rarely reported.

In this study, we prepared an amphiphilic block polymer-based dual-modality contrast agent Gd-DOTA-TPBP for MRI and FI. Within this agent, Gd-DOTA was used as a MRI probe and TPBP as a two-photon excitation FI probe. Its structure and function were schematically shown in Scheme 1. In this contrast agent, Gd-DOTA and TPBP were covalently attached to hydrophilic and hydrophobic chain segments of the polymer, respectively, with high stability. This amphiphilic block polymer could self-assemble into a micelle due to hydrophilic and hydrophobic interaction. Gd-DOTA was located in the exterior of the hydrophilic shell, which could sufficiently interact with water molecules to maintain its relaxivity. Meanwhile, TPBP was wrapped in a hydrophobic core to result in an enhancement in the fluorescence signal intensity due to its AIE property, and its tissue penetration depth could reach more than 100 μm in the two-photon excitation mode. Gd-DOTA-TPBP could serve as a contrast agent for both MRI and FI *in vitro* and *in vivo* to obtain complementary microscopic and macroscopic information of normal and tumor tissues.

2. Experimental methods

2.1. Materials and measurements

Azidobenzoic acid, benzoyl chloride, DBCO-acid, *N,N′*-Dicyclohexylcarbodiimide (DCC), Oligo(ethylene glycol) methyl ether methacrylate (OEGMA, Mw ≈ 500 Da), 4-(dimethylamino)pyridine (DMAP) were purchased from Aladdin Reagent Co., Ltd. (Shang Hai, China). 4-cyanopentanoic acid dithiobenzoate (CTA) and $GdCl_3{\cdot}6H_2O$ were acquired from Sigma-Aldrich (St. Louis., MO, USA). All other chemicals and reagents were purchased from Kelong Chemicals (Chengdu, China) and used without further purification. TPBP-OH [28], the monomer HPMA [29], MA-DOTA [30] and the macromolecular chain transfer agent, p(DOTA-co-pOEG)-CTA [31], were synthesized according to previously reported methods.

^{1}H NMR and ^{13}C NMR spectra were recorded using a Bruker Advance 400 MHz spectrometer. High-resolution mass spectrometry (HRMS) spectral data were obtained using a Bruker Daltonics Bio TOF mass spectrometer. Gel permeation chromatography (GPC; Shimadzu, Japan) was used to measure the polymer molecular weight. The hydrodynamic diameter of polymeric conjugate was measured by dynamic light scattering (DLS) on a NanoBrook Omni (Brookhaven Instruments, New York, USA). The morphology of nanoparticles was observed under a transmission electron microscopy (TEM, Tecnai GF20S-TWIN, USA). The Gd(III) content in polymers was measured via inductively coupled plasma atomic emission spectroscopy (ICP-AES, Agilent 5100, USA). The TPBP content in polymers was determined via a UV–Vis spectroscope (Shimadzu, UV1800ENG240V, SOFT, Japan). The absolute fluorescence quantum yields were detected on a Horiba Fluorolog-3 fluorescence spectrometer with a calibrated integrating sphere system (Horiba, Fluorolog-3, USA).

2.2. Synthesis of HPMA-Bz

First, HPMA (0.80 g, 5.59 mmol) was dissolved in 20 mL tetrahydrofuran (THF) in a round bottom flask. Subsequently, triethylamine (1.17 mL, 8.38 mmol) and a catalytic amount of DMAP were added

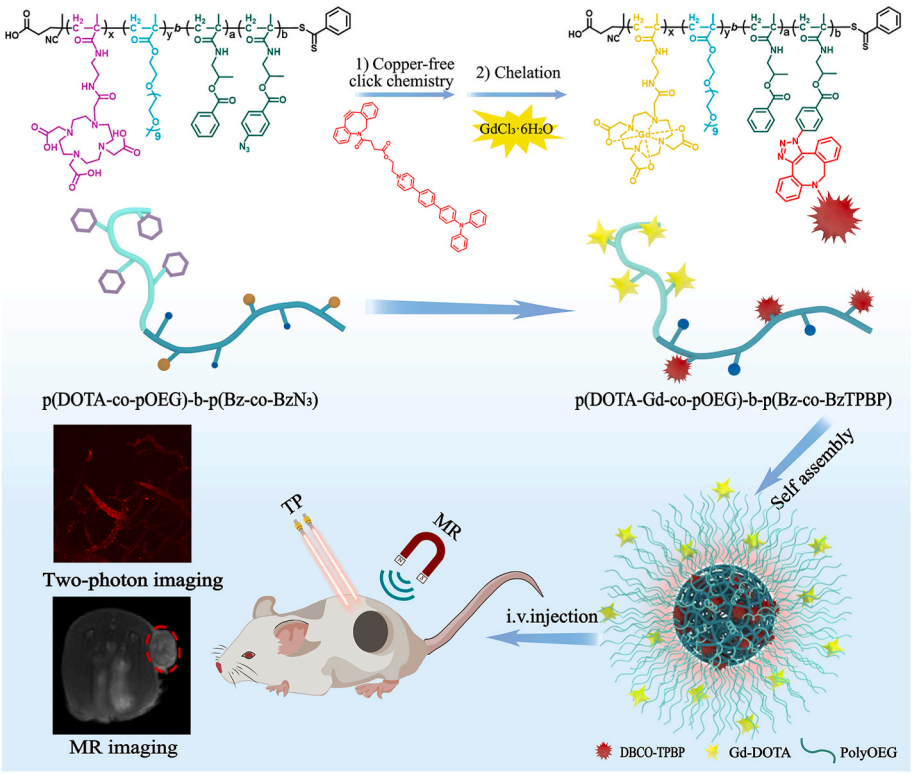

Scheme 1. Schematic diagram for synthesis of an imaging probe, Gd-DOTA-TPBP, for magnetic resonance imaging (MRI) and two-photon fluorescent imaging (TPFI) after stepwise copper-free click chemistry and chelation. The amphiphilic block conjugate Gd-DOTA-TPBP could self-assemble to form stable nanoparticles for dual-modality imaging of mice with high sensitivity.

under an ice bath. After stirring for 10 min, 20 mL of the THF solution containing benzoyl chloride (1.17 g, 8.38 mmol) was added dropwise, and the reaction continued for 12 h. After the reaction was completed, triethylamine hydrochloride was removed by filtration, and the filtrate was distilled under a reduced pressure to remove the solvent. The obtained crude product was further purified by silica gel column chromatography. Finally, 1.12 g of a white solid product HPMA-Bz was obtained with a yield of 81%.

2.3. Synthesis of HPMA-BzN_3

HPMA (0.20 g, 1.40 mmol), azidobenzoic acid (227.87 mg, 1.40 mmol), DMAP (51.29 mg, 0.42 mmol) and DCC (433.29 mg, 2.10 mmol) were dissolved in 20 mL dichloromethane (DCM) in an ice bath, and the mixture was stirred for 6 h at 0 °C. After the reaction is completed, the solution was removed by rotary evaporation, and 20 mL of ethyl acetate was added to the residue, and placed in the refrigerator overnight to precipitate the majority of 1, 3-dicyclohexylurea (DCU). After filtration, the filtrate was evaporated to remove the solvent, and the residue was subjected to silica gel column chromatography to obtain 252 mg of pale yellow solid, HPMA-BzN_3, with a yield of 63%.

2.4. Synthesis of TPBP-DBCO

TPBP-OH (100.00 mg, 0.17 mmol), DBCO-acid (47.16 mg, 0.15 mmol), DMAP (10.38 mg, 0.09 mmol) and DCC (56.61 mg, 0.26 mmol) were dissolved in 12 mL of a mixed solution (DMF:DCM = 1:5, v/v) in an ice bath, and the mixture was stirred for 6 h at 0 °C. After the reaction is completed, the reaction solution was washed with deionized water, HCl (0.1 M) and $NaHCO_3$ aq. (satd.), respectively, then dried with $MgSO_4$. $MgSO_4$ was removed by filtration, and the solvents were removed by rotary evaporation. The residue was dissolved in 10 mL ethyl acetate and placed in the refrigerator overnight to precipitate the majority of DCU. After filtration, the filtrate was evaporated to remove the solvent, and then residue was subjected to silica gel column chromatography to obtain 65 mg of orange yellow solid, TPBP-DBCO, with a yield of 44%.

2.5. Synthesis of polymer p(DOTA-co-pOEG)-b-p(Bz-co-BzN_3)

To prepare an amphiphilic block polymer, a macromolecular chain transfer agent, p(DOTA-*co*-pOEG)-CTA, was first prepared by a slightly modified method in a previous report [30]. Briefly, MA-DOTA (2.00 g, 2.06 mmol), OEGMA (0.61 g, 1.21 mmol), 4-cyanopentanoic acid dithiobenzoate (CTA, 36.3 mg, 0.13 mmol) and an initiator, 4,4′-azobis (4-cyanovaleric acid) (ACVA, 10.93 mg, 39 μmol), were placed in a 15 mL vial. Subsequently, 10 mL of a trifluoroethanol (TFE) solution was added into the vial under an argon atmosphere. After bubbling with argon for 0.5 h in an ice bath, the vial was transferred to an oil bath at 73 °C. After the reaction solution was stirred for 24 h in the dark, it was quenched with liquid nitrogen. The crude product was purified by dialysis and freeze-dried to yield p(DOTA-*co*-OEG)-CTA.

In the second RAFT polymerization, p(DOTA-*co*-pOEG)-CTA (500 mg, ~55.4 μmol), HPMA-Bz (429.58 mg, 1.74 mmol), HPMA-BzN_3 (93.92 mg, 0.35 mmol) and ACVA (3.66 mg, 13.04 μmol), were placed in a 10 mL vial. Subsequently, under an argon atmosphere, 4 mL of TFE solution was added into the vial. After bubbling with argon for 0.5 h in an ice bath, the vial was transferred to an oil bath at 73 °C with stirring for 24 h in the dark. Thereafter, the polymerization was quenched with liquid nitrogen. Subsequently, 2 mL of DCM was added to the reaction solution. The reaction solution was added dropwise to ether. The precipitated solid was collected and re-dissolved in a mixed solution of DCM/methanol. After ether was added to the mixed solution, the precipitate was collected and dried in vacuum to obtain 581 mg of a pink solid product with a yield of 57%.

2.6. Synthesis of polymer p(DOTA-co-pOEG)-b-p(Bz-co-BzTPBP)

The polymer p(DOTA-*co*-pOEG)-*b*-p(Bz-*co*-BzN_3) (500 mg) was dissolved in a mixed solution of methanol and DCM (5 mL, volume ratio 1:1), and TPBP-DBCO (30 mg) was then added. The reaction solution was stirred at room temperature for 24 h. Thereafter, the reaction solution was added dropwise to 200 mL of ether, and the precipitate was collected by centrifugation. After drying, 523 mg of an orange-yellow solid product was obtained with a yield of 98%.

2.7. Synthesis of polymer Gd-p(DOTA-co-pOEG)-b-p(Bz-co-BzTPBP)

The polymer p(DOTA-*co*-pOEG)-*b*-p(Bz-*co*-BzTPBP) (465 mg) and $GdCl_3{\cdot}6H_2O$ (465 mg) were dissolved in 30 mL of deionized water. Subsequently, NaOH (0.1 M) was used to adjust the pH of the reaction solution to 5.2–5.4, and the reaction continued within this pH range for 24 h. Finally, the reaction solution was dialyzed (MWCO: 3.5 kDa) with deionized water to remove excess Gd(III). The dialysis solution was lyophilized to obtain orange-yellow fluffy solid, Gd-p(DOTA-*co*-pOEG)-*b*-p(Bz-*co*-BzTPBP) (486 mg).

2.8. AIE effect measurement

Gd-DOTA-TPBP was dissolved in a series of mixed solutions (deionized water: DMSO = 100:0, 90:10, 70:30, 50:50, 30:70, 10:90 and 0:100, respectively). The fluorescence intensity of the solutions was measured via a fluorescence spectrophotometer (Hitachi, Japan, excitation 410 nm, emission 450–810 nm).

2.9. Critical micelle concentration (CMC) measurement

Gd-DOTA-TPBP was dissolved in deionized water with gradient concentrations (0–1000 μg/mL). A pyrene solution was prepared by dissolving pyrene in acetone at a concentration of 10 μg/mL. The pyrene/acetone solution (21 μL) was transferred into an EP tube and the tube was placed in a ventilated dark place to allow acetone to evaporate completely. The Gd-DOTA-TPBP solution with different concentrations were then added to the EP tube with pyrene and incubated overnight at 37 °C. Finally, the fluorescence intensity of the mixture was measured via a fluorescence spectrophotometer. The fluorescence excitation wavelength was 330 nm and the emission wavelength range was from 350 to 450 nm. The I_1 and I_3 were the peak values at $\lambda_1 = 372$ nm and $\lambda_3 = 383$ nm respectively, and the I_1/I_3 ratio was calculated. The CMC value was calculated from the I_1/I_3 values at different concentrations.

2.10. Relaxivity measurement

Gd-DOTA-TPBP was dissolved in the PBS solution to prepare Gd(III) solutions at a Gd(III) concentration of 0, 0.05, 0.10, 0.15, 0.20, 0.25, 0.30, 0.35, 0.40, 0.45 and 0.50 mM. Gd-DTPA, the most commonly used small molecular MRI contrast agent in clinic, was set as a control. The relaxivity scanning was performed via a clinical magnetic resonance scanner (3.0 T trio, Siemens, Germany), and T_1-weighted MR images were acquired with a series of spin echo (SE) sequences. The slope of the linear fit between $1/T_1$ versus the Gd(III) concentration was the r_1 value of the contrast agent.

2.11. Cell culture

HUVECs (Human Umbilical Vein Endothelial Cells), LO2 cells (Human liver cells) and 4T1 cells from a mouse breast cancer cell line were supplied from the Cell Bank of the Chinese Academy of Sciences (Shanghai, China). The DMEM medium was used to culture HUVECs and LO2 cells, and 1640 medium for 4T1 cells. The cells out of the liquid nitrogen tank were passaged at least twice for experimental use.

2.12. Cytotoxicity assessment

HUVECs, 4T1 cells and LO2 cells were seeded in 96-well plates and cultured in a normal oxygen incubator (5% CO_2, 37 °C). After 24 h, Gd-DOTA-TPBP, Gd-DTPA or TPBP at an equivalent Gd(III) concentration of 0–200 μg/mL or a TPBP concentration of 0–69 μg/mL was added in each well (n = 5 for each group). After the cells were incubated with contrast agents for 24 h, the CCK8 (MedChemExpress, USA) assay was performed to measure the cytotoxicity of experimental and control groups.

2.13. Hemolysis measurement

Two mL of blood was withdrawn from healthy 8–10 week old BALB/c female mice and collected in an EP tube which was infiltrated with heparin. The blood was centrifuged (1000 g, 4 °C) for 5 min, and the upper serum was removed and red blood cells (RBCs) at the bottom were collected. The RBCs were then suspended in the PBS solution to make a 20% RBC suspension. Next, 1 mL of the Gd-DOTA-TPBP solution was added to 50 μL of the RBC suspension, and the final concentrations of the contrast agent were 1, 2 and 5 mg/mL (n = 3 for each group). H_2O was set as the positive control, PBS as the negative control, and Gd-DTPA diluted by PBS as a control. The mixture was incubated at 37 °C for 24 h, and the RBC suspensions were then centrifuged. The final supernatant was collected for absorbance reading (Bio Tek, EON, USA). The hemolysis % calculation was performed via the formula reported previously [7].

2.14. Animal model establishment

Healthy female BALB/c mice (8–10 week-old, 20 ± 2 g, Chengdu Dossy Experimental Animals Co., Ltd) were used to establish a subcutaneous 4T1 tumor model. 4T1 cells were cultured and collected. After they were rinsed with PBS three times, they were re-suspended with cold PBS. 1×10^6 4T1 cells were inoculated under the side back skin of mice. All animal procedures were performed in accordance with the Guidelines for Care and Use of Laboratory Animals of West China Hospital, Sichuan University (No. 2018148A and 2018150A).

2.15. MR imaging in vivo

Healthy female BALB/c mice (8-10 week-old, 20 ± 2 g) were randomly divided into 2 groups for brain MR angiography (n = 3 for each group), while animal models with 4T1 tumors were randomly divided into 2 groups for tumor MR angiography (n = 3 for each group) when the diameter of the tumor was between 5 and 10 mm. Gd-DOTA-TPBP and Gd-DTPA was diluted with PBS and injected to mice through tail veins at 0.1 mmol Gd(III)/kg, and the MR images were acquired before injection (pre), 10 min, 45 min, 2 h and 3.5 h post injection. The Bruker 7.0T animal MRI scanner was used for scanning, and the scanning parameters were, TR: 5.5 ms; TE: 2.6 ms; voxel size: 0.12 × 0.12 × 0.35 mm^3; and Fov: 35 × 35 × 45 mm.

Another six mice with 4T1 tumors were randomly divided into 2 groups for tumor contrast enhanced MR imaging when the diameter of the tumor was between 5 and 10 mm. Gd-DOTA-TPBP and Gd-DTPA was diluted with PBS and injected to mice through tail veins at 0.08 mmol Gd(III)/kg, and the MR images were acquired before injection (pre), 10 min, 45 min, 1.5 h, 2.5 h, 4 h and 8 h post injection. The Siemens 3.0 T clinical MRI scanner (Trio) equipped with a mouse coil (Shanghai Chenguang Medical Technology Co., Ltd.) was used for scanning, and the scanning parameters were, TR: 350 ms; TE: 12 ms; Slices: 10; voxel size: 0.2 × 0.2 × 1.0 mm^3; and Fov: 45 × 45 mm.

MR imaging of main organs (liver, kidney and bladder) were applied on 8-week old BALB/c female mice (n = 3 for each group). All the procedures were the same as that for tumor contrast enhanced MR imaging, but the scanning parameters were changed to, TR: 500 ms; TE: 11 ms; Slices: 13; voxel size: 0.2 × 0.2 × 3.3 mm^3; and Fov: 47 × 47 mm.

RadiAnt DICOM Viewer was used to analysis MR images and acquire the value of signal intensity in region of interest.

2.16. Confocal fluorescence imaging in vivo

Animal models at the tumor diameters between 5 mm and 10 mm were chosen for *in vivo* confocal fluorescence imaging (n = 3 for each group). Gd-DOTA-TPBP was diluted with PBS and injected to mice through tail vein at 8 mg TPBP/kg, and the mice were then anesthetized by isoflurane and positioned in a prone position with the brain or the tumor in contact with a coverslip mounted on the stage of a two photon confocal microscope (Nikon, A1RMP+). The images of the brain were photographed at 90 min after injection of Gd-DOTA-TPBP, and those of the tumor at 90 min and 24 h after injection. The excitation wavelength was 800 nm and the emission wavelength was at the range from 580 to 620 nm. Confocal fluorescence images were analyzed by NIS-Elements Viewer.

2.17. Statistical analyses

Comparison between datasets was carried out by two-tailed *t*-test for statistical significance. The difference was considered to be statistically significant with a p value of <0.05 or very significant with a *p* value of <0.01.

3. Results and discussion

3.1. Preparation and characterization of amphiphilic polymers

We designed and prepared an amphiphilic polymer as a magnetic resonance/fluorescence dual-modality contrast agent, Gd-p(DOTA-*co*-pOEG)-*b*-p(Bz-*co*-BzTPBP) (Gd-DOTA-TPBP). The intermediates and the final polymer were synthesized according to the routes shown in Schemes S1 and S2. First, a hydrophilic macromolecular chain transfer agent, p(DOTA-*co*-pOEG)-CTA, was prepared by copolymerizing OEGMA, MA-DOTA and CTA by RAFT polymerization. To obtain amphiphilic polymers, hydrophobic compounds, HPMA-Bz, HPMA-BzN_3 and BPTP-DBCO, were synthesized and their chemical structures were confirmed via ^{1}H NMR and high-resolution mass spectrometry (HRMS) (Figs. S1–S9, Supporting Information). Subsequently, p(DOTA-*co*-pOEG)-CTA was copolymerized with HPMA-Bz and HPMA-BzN_3 to obtain an amphiphilic block polymer, p(DOTA-*co*-pOEG)-*b*-p(Bz-*co*-BzN_3). Due to the presence of azide groups in the hydrophobic segment, TPBP-DBCO, a two-photon fluorescent probe, could be conjugated to p(DOTA-*co*-pOEG)-*b*-p(Bz-*co*-BzN_3) through copper-free click reaction to yield the polymer, p(DOTA-*co*-pOEG)-*b*-p(Bz-*co*-BzTPBP). Finally, in a weakly acidic environment, $GdCl_3{\cdot}6H_2O$ was chelated with the DOTA groups in p(DOTA-*co*-pOEG)-*b*-p(Bz-co-BzTPBP) to form Gd-DOTA, and a stable magnetic resonance/fluorescence dual-modal contrast agent, Gd-p(DOTA-*co*-pOEG)-*b*-p(Bz-*co*-BzTPBP) (Gd-DOTA-TPBP), was obtained.

The chemical structures of Gd-DOTA-TPBP and its intermediate products were confirmed via ^{1}H NMR, GPC, fourier transform infrared (FTIR) analysis and energy dispersive X-ray spectroscopy (EDX). As shown in Fig. S10, in the ^{1}H NMR spectrum of p(DOTA-*co*-pOEG)-CTA, characteristic peaks of DOTA (3.62–3.16 ppm), OEG (4.18 ppm and 3.70 ppm) and CTA (7.96 ppm, 7.70 ppm, 7.54 ppm) were observed, indicating that a hydrophilic macromolecular chain transfer agent was successfully prepared. Compared with the ^{1}H NMR spectrum of p(DOTA-*co*-pOEG)-CTA, characteristic peaks of benzene in the aromatic region was found at 8.01–7.44 ppm in the ^{1}H NMR spectrum of p(DOTA-*co*-pOEG)-*b*-p(Bz-*co*-BzN_3), indicating that the monomers containing the benzene ring were successfully introduced into the polymer backbone through copolymerization (Fig. S11). Furthermore, a broad aromatic region (7.99–7.07 ppm) was observed in the ^{1}H NMR spectrum of p(DOTA-*co*-pOEG)-*b*-p(Bz-*co*-BzTPBP), and the peak area ratio of the aromatic region increased compared to that of p(DOTA-*co*-pOEG)-*b*-p(Bz-*co*-BzN_3), indicating that TPBP was successfully coupled to the polymer side chain (Fig. 1. A). FTIR spectroscopy (Fig. 1B) also supported successful conversion of azide groups in p(DOTA-*co*-pOEG)-*b*-p(Bz-*co*-BzN_3). After the click reaction, the characteristic resonance of $-N_3$ on p(DOTA-*co*-pOEG)-*b*-p(Bz-*co*-BzTPBP) at 2100 cm^{-1} disappeared (Fig. 1. B), indicating that TPBP was coupled to the polymer through the click reaction of alkynyl and azide [32]. Furthermore, a characteristic peak of TPBP (410 nm) was observed in the UV–vis spectrum of p(DOTA-*co*-pOEG)-*b*-p(Bz-*co*-BzTPBP) compared to the unlabled polymer p(DOTA-OEG)-*b*-p(BzN_3) (Fig. 1. C), confirming TPBP was successfully covalently coupled to the unlabeled polymer. The results of GPC analysis showed that p(DOTA-*co*-pOEG)-*b*-p(Bz-*co*-BzTPBP) obtained after further RAFT polymerization had a high molecular weight (12.9 kDa) and a narrow polydispersity (PDI = 1.40), further indicating that we successfully prepared amphiphilic block polymers by using p(DOTA-*co*-pOEG)-CTA as chain transfer agent (Fig. S12). After chelating Gd(III), we analyzed the elements in Gd-p(DOTA-*co*-pOEG)-*b*-p(Bz-*co*-BzTPBP) by EDX. As shown in Fig. 1D, the conjugate contained N, S, O, and Gd elements, indicating that Gd ions were successfully chelated into the polymer. Furthermore, the gadolinium content in Gd-p(DOTA-*co*-pOEG)-*b*-p(Bz-*co*-BzTPBP) measured via ICP-AES was 13.8%, and the load of TPBP measured via a UV–vis spectrophotometer was 4.8%. The above results supported that the amphiphilic polymer-based magnetic resonance/fluorescence dual-modal contrast agent, Gd-DOTA-TPBP, was successfully synthesized. It is worth noting that although polymer-based MRI/FI dual-modality contrast agents have been reported, very few of these contrast agents are able to balance controllability, biocompatibility and stability [33–35]. Gd-DOTA-TPBP was prepared from OEGMA and HPMA derivatives by controllable RAFT polymerization and efficient copper-free click chemistry, thus it had great biocompatibility and structural controllability. Meanwhile, both Gd-DOTA and TPBP were incorporated to the polymer backbone through covalent bonds, which could help maintaining the stability of Gd-DOTA-TPBP during *in vivo* circulation. In addition, the fluorescent probe TPBP, a model molecule for FI, has a two-photon AIE effect, thus it could effectively prevent the ACQ effect of traditional fluorescent molecules. Therefore, Gd-DOTA-TPBP derived from amphiphilic block polymers may have unique advantages in its physicochemical properties and biological functions compared with traditional polymer-based MRI/FI dual-modality contrast agents and it may have excellent performance in the field of bioimaging.

3.2. Characterization of self-assembly nanoparticles

The self-assembly behavior of Gd-DOTA-TPBP in an aqueous solution was first investigated, due to its amphiphilic block structure. The contrast agent, Gd-DOTA-TPBP, was amphiphilic, and it self-assembled to form micelles in an aqueous solution. The CMC value of Gd-DOTA-TPBP was 12.86 μg/mL (Fig. 1E). Since the blood concentration of the contrast agent for MR or fluorescence imaging was much higher than its CMC value, which indicated Gd-DOTA-TPBP could self-assemble into stable micelles for its *in vivo* application.

The fluorescence quantum yields of TPBP and Gd-DOTA-TPBP at different states were calculated and summarized in Table S1. Solid TPBP displayed a strong emission at 613 nm with a fluorescence quantum yield of 11.3%, while its DMSO solution displayed a weak emission with a fluorescence quantum yield of 0.1% at the same wavelength. Gd-DOTA-TPBP had a slightly higher quantum yield in a solid state with a Φ_f of 13.1% and a Φ_f of 0.4% in DMSO in comparison with TPBP. Subsequently, the AIE property of Gd-DOTA-TPBP was investigated. To measure the AIE index of Gd-DOTA-TPBP, its aqueous solution was mixed with an organic solvent, DMSO, at different ratios to monitor the changes in the fluorescence intensity of Gd-DOTA-TPBP. Fig. 1F showed that the fluorescence intensity of the contrast agent was highest when the ratio of water to DMSO was 90:10–100:0. As the ratio of DMSO to

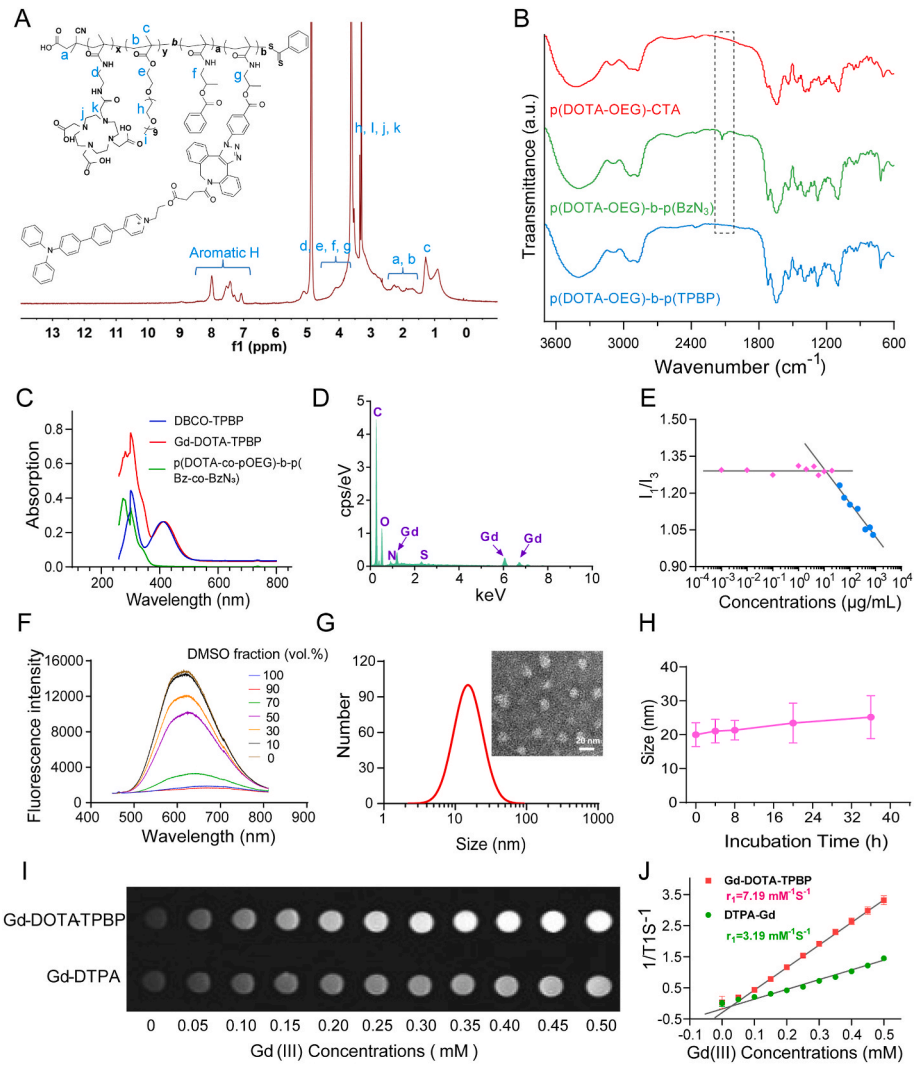

Fig. 1. Physicochemical characterizations of Gd-DOTA-TPBP. (A) ^{1}H NMR spectrum of p(DOTA-OEG)-*b*-p(TPBP) in CD_3OD. (B) FTIR spectra of p(DOTA-OEG)-CTA, p(DOTA-OEG)-*b*-p(BzN_3) and p(DOTA-OEG)-*b*-p(TPBP). (C) Absorbance spectra of TPBP, Gd-DOTA-TPBP, and p(DOTA-OEG)-*b*-p(BzN_3). (D) EDX spectrum of Gd-DOTA-TPBP. The peak for each element is assigned from the standard references. (E) Critical micelle concentration (CMC) of Gd-DOTA-TPBP using pyrene as a fluorescence probe. (F) Fluorescent spectra of Gd-DOTA-TPBP at different ratios of DMSO/water. (G) Typical TEM image and hydrodynamic size of Gd-DOTA-TPBP nanoparticles measured by dynamic light scattering (DLS). (H) The stability results of Gd-DOTA-TPBP in PBS (pH 7.4) for 36 h. (I) T_1-weighted MR images of Gd-DOTA-TPBP in PBS at different Gd(III) concentrations. (J) Water proton longitudinal relaxation rate ($1/T_1$) versus the Gd(III) concentration of Gd-DTPA and Gd-DOTA-TPBP conjugates in PBS in a field of 3.0 T.

water increased, the fluorescence intensity of the contrast agent decreased. When the ratio of DMSO to water was as high as 90%–100%, the fluorescence intensity of Gd-DOTA-TPBP was barely detectable. In an aqueous solution, TPBP was wrapped inside Gd-DOTA-TPBP and it aggregated to emit strong fluorescence signal. On the contrary, Gd-DOTA-TPBP was not able to assemble in an organic solvent. Therefore, the level of molecular aggression decreased with an increase in the DMSO concentration. Those results supported that Gd-DOTA-TPBP could be self-assembled into micelles with a hydrophobic core.

To determine the hydrodynamic size of Gd-DOTA-TPBP, the polymer solution at a final concentration of 300 μg/mL was prepared. Fig. 1G displayed that the hydrodynamic size of Gd-DOTA-TPBP was about 20 nm. Previous studies have shown that when the hydrodynamic size of a drug delivery system is greater than 20 nm, it can not be rapidly cleared by the kidney during the circulation [36], resulting in a prolonged circulation time. Such a long blood circulation time would be beneficial for angiography via the contrast agent. Meanwhile, the hydrodynamic size facilitated the contrast agent to accumulate at the tumor site through the enhanced permeability and retention (EPR) effect, resulting in significant improvement in the imaging contrast between tumors and normal tissues/organs, and a distinguished boundary of tumors for identification and diagnosis of tumors. A spherical morphology of Gd-DOTA-TPBP was shown in Fig. 1G under a TEM. This result supported that Gd-DOTA-TPBP could self-assemble to micelles in water, and maintain its morphology after drying. In addition, the changes in the hydrodynamic size of Gd-DOTA-TPBP in PBS were recorded at different time points and Fig. 1H showed that the hydrodynamic sizes of Gd-DOTA-TPBP had no significant change within the incubation time, indicated Gd-DOTA-TPBP could be stable in H_2O for at least 36 h.

3.3. Relaxivity measurements

Fig. 1I showed that the MRI signals of Gd-DOTA-TPBP and Gd-DTPA increased with an increase in the gadolinium concentration, and the MRI signal intensity of Gd-DOTA-TPBP was higher than that of Gd-DTPA at the same gadolinium concentration. Those results indicated that Gd-DOTA-TPBP may have a higher relaxivity than Gd-DTPA. The r_1 value of the contrast agent was calculated (Fig. 1J) and the r_1 value of Gd-DOTA-TPBP was 7.19 $mM^{-1}S^{-1}$, which was significantly higher than that of Gd-DTPA (3.19 $mM^{-1}S^{-1}$). This result also supported that Gd-DOTA-TPBP had a higher relaxivity than Gd-DTPA. According to the Solomon-Bloembergen-Morgan principle, a slow tumbling rate is an important characteristic parameter of a T_1 contrast agent with a high relaxivity [18]. Previous studies suggest that a high molecular weight of polymeric contrast agents contributes to the improvement in the relaxivity because the presence of high-MW polymers could slow down the tumbling rate [7,30]. Therefore, a higher r_1 value of Gd-DOTA-TPBP could be ascribed to its high MW.

3.4. Cell uptake and cytotoxicity of Gd-DOTA-TPBP

HUVECs and 4T1 cells were used to assess cellular uptake of Gd-DOTA-TPBP. After culture with Gd-DOTA-TPBP for 2 h, 4T1 cells and HUVECs exhibited strong red fluorescence under two-photon excitation as shown in Fig. 2A and Fig. 2B. After 4 h incubation, the intracellular fluorescence intensity became evidently stronger. Those results indicated that Gd-DOTA-TPBP was able to enter both tumor and somatic cells in a time-dependent manner, and it could be used for two-photon excitation fluorescence imaging of cells *in vitro*. Furthermore, we evaluated the MR contrast-enhanced imaging performance of Gd-DOTA-TPBP. After treating 4T1 cells with Gd-DTPA and Gd-DOTA-TPBP, stronger MR signal intensity was observed in the cells treated with Gd-DOTA-TPBP compared with Gd-DTPA-treated cells at the equivalent Gd(III) concentrations (Fig. S13). Such strong MR signal of Gd-DOTA-TPBP could be ascribed to its high relaxivity. These results indicated that Gd-DOTA-TPBP could be used as a contrast-enhanced MR imaging agent for cells *in vitro* and it had a better contrast enhancement effect than Gd-DTPA.

HUVECs, 4T1 cells and LO2 cells were used to measure the cytotoxicity of Gd-DOTA-TPBP, Gd-DTPA and TPBP (n = 5 for each group). Fig. 2C, D and Fig. S14 showed after incubation with the cells for 24 h, the cell viability in Gd-DOTA-TPBP-treated groups was more than 90% at the highest Gd(III) concentration (200 μg/mL), which indicated Gd-DOTA-TPBP did not induce toxicity to the three cell lines. Similar observations were applied to Gd-DTPA. However, TPBP induced pronounced toxicity to all cell lines even at a low concentration. Those results suggested Gd-DOTA-TPBP exhibited minor toxicity to 4T1 cells, HUVECs and LO2 cells, and the cytotoxicity of TPBP could be significantly reduced by covalent binding of the fluorophore to a polymeric backbone.

3.5. Toxicity assessment in vivo

Hemolysis induced by Gd-DOTA-TPBP was also assessed before it was injected into animals through tail vein for *in vivo* application (n = 3 for each group). After red blood cells were incubated with different solutions overnight (Fig. 2E), the supernatant in the groups treated with PBS, Gd-DTPA and Gd-DOTA-TPBP retained its original color. However, the supernatant in the group treated with H_2O changed to red. The UV absorbance at 504 nm of the supernatant was read and the hemolysis rate for each group was calculated. Fig. 2F showed at a concentration of Gd-DOTA-TPBP of 1 mg/mL, 2 mg/mL or 5 mg/mL, the hemolysis rate was lower than 2%. According to the ASTM standards [30], when the hemolysis rate is less than 5%, the sample is highly hemocompatible. Such a low hemolysis rate of Gd-DOTA-TPBP suggested it could be

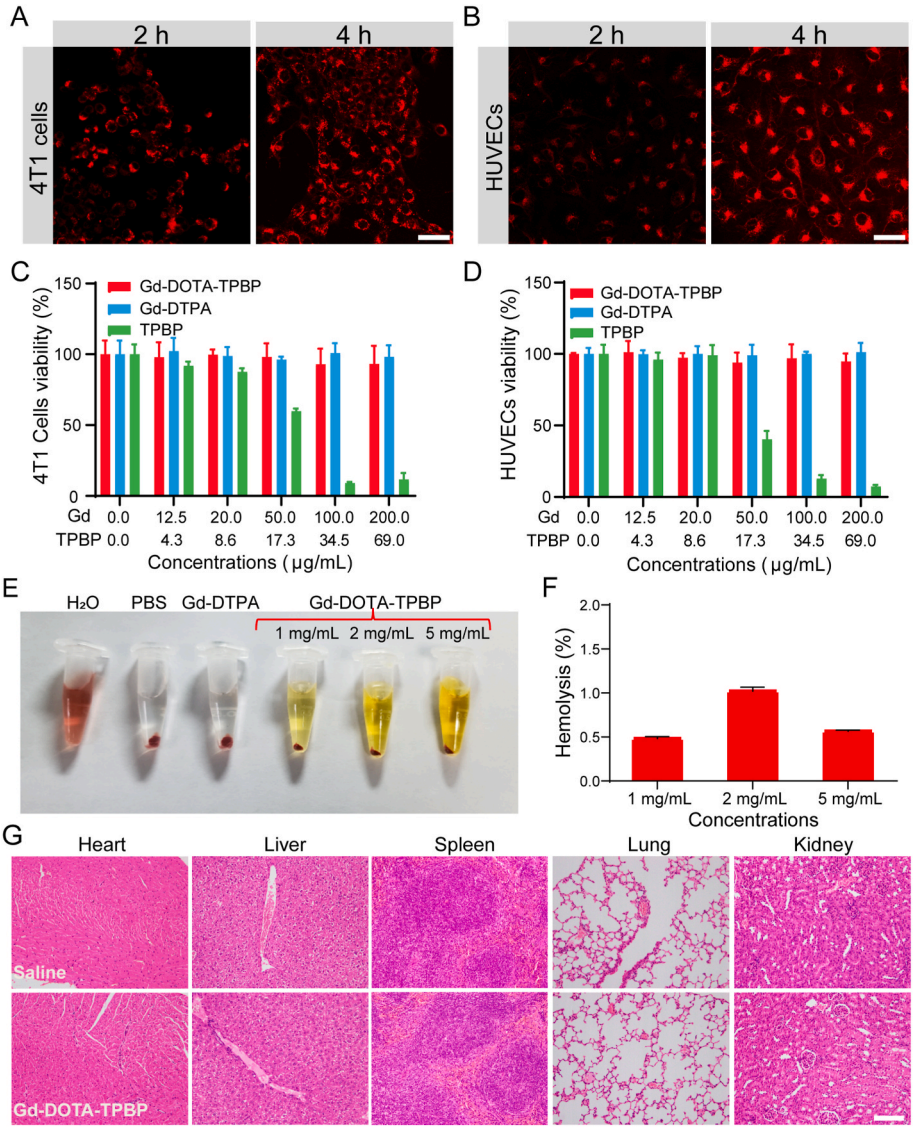

Fig. 2. Cellular uptake, cell viability and toxicity assessment of Gd-DOTA-TPBP. (A) Two-photon CLSM images of 4T1 cells cultured with Gd-DOTA-TPBP for different durations excited at 800 nm. (B) Two-photon CLSM images of HUVECs cultured with Gd-DOTA-TPBP for different durations excited at 800 nm. The scale bar is 50 μm. (C) Viability of 4T1 cells cultured with Gd-DOTA-TPBP, Gd-DTPA or TPBP at different Gd(III) or TPBP concentrations for 24 h (n = 5). (D) Viability of HUVECs cultured with Gd-DOTA-TPBP, Gd-DTPA or TPBP at different Gd(III) or TPBP concentrations for 24 h (n = 5). (E) Photos of red blood cells incubated with different solutions for 24 h after centrifugation. (F) Hemolysis rates of Gd-DOTA-TPBP at different concentrations (n = 3). (G) H&E analysis of different organs at 24 h post-injection of Gd-DOTA-TPBP or saline. The scale bar is 100 μm.

injected to animal models through the blood circulation system.

To further evaluate the toxicity of the contrast agent *in vivo*, Gd-DOTA-TPBP (0.1 mmol Gd(III)/kg) or saline was intravenously injected to healthy BALB/c female mice. Main organs of the mice were collected to prepare histological sections for H&E analysis at 24 h post injection. Fig. 2G displayed that there were no significant edema, hemorrhage, inflammatory cell infiltration, necrosis or other pathological signs in both Gd-DOTA-TPBP-treated or saline-treated groups, indicating that Gd-DOTA-TPBP would not induce acute toxicity to tissues and organs *in vivo*.

3.6. Vascular imaging in vivo

3.6.1. MR angiography

An animal 7.0 T MRI scanner was employed to evaluate the contrast-enhanced effect when Gd-DOTA-TPBP was used for angiography, and Gd-DTPA was used as a control (n = 3 for each group). MR angiography of mouse brains was shown in Fig. 3A. At 10 min post injection of Gd-DOTA-TPBP, contrast enhancements were seen in bilateral internal carotid arteries, anterior and middle cerebral arteries, basilar arteries and their branches, and these enhancements peaked at 45 min post injection. At 2 h post injection, the enhancement degree in intracranial and external vessels decreased, meanwhile the lumen filling degree decreased, and the number of visible branches of large vessels reduced. At 3.5 h after injection, the enhancement degree in intracranial and external vessels was further decreased but the signal was still detectable. On the contrary, in the Gd-DTPA-treated group (Fig. 3A), the signal in intracranial bilateral middle and anterior cerebral arteries was slightly enhanced at 10 min post injection, and sparse visible branches were observed. There was no obvious MR signal enhancement in these arteries after 45 min post injection. The experimental results strongly supported that Gd-DOTA-TPBP outperformed clinical Gd-DTPA in MR angiography of normal mouse heads, such as a high degree of enhancement, clear and distinguishable vascular anatomical details, and a long duration of enhancement.

Fig. 3B demonstrated that Gd-DOTA-TPBP also performed well in contrast-enhanced MR angiography of peritumoral blood vessels in the mice treated with Gd-DOTA-TPBP. The peritumoral blood vessels were not visible before injection of the contrast agent. After 10 min post injection, the MR signal in peritumoral blood vessels was significantly boosted and the signal lasted up to 2 h post injection. In contrast, the blood vessels in the Gd-DTPA-treated group were only visible at 10 min post injection, and the duration for contrast enhancement was short and the contrast in soft tissues was poor. Compared with Gd-DTPA, injection of Gd-DOTA-TPBP allowed a longer time for visualization of tumor blood supply vessels with a higher enhancement level. A higher relaxivity and a longer blood circulation time of Gd-DOTA-TPBP could contribute to its outstanding performance in MR angiography.

3.6.2. Two-photon excitation confocal microscopy imaging

Although MR angiography with Gd-DOTA-TPBP as a contrast agent had a longer imaging time and revealed more details compared to Gd-DTPA, the imaging resolution for micro blood vessels was insufficient. The blood vessels inside the tumor was not be able to be clearly seen even when a 7.0 T MR scanner was chosen, while peritumoral blood vessels could be clearly revealed from this contrast agent. A high resolution of confocal fluorescence microscopy allows observation of micro blood vessels and cell-level structures, which can be a complement to MRI angiography [37], especially in tumor angiography. The use of dual-modal contrast agents for MR and confocal fluorescence *in vivo*

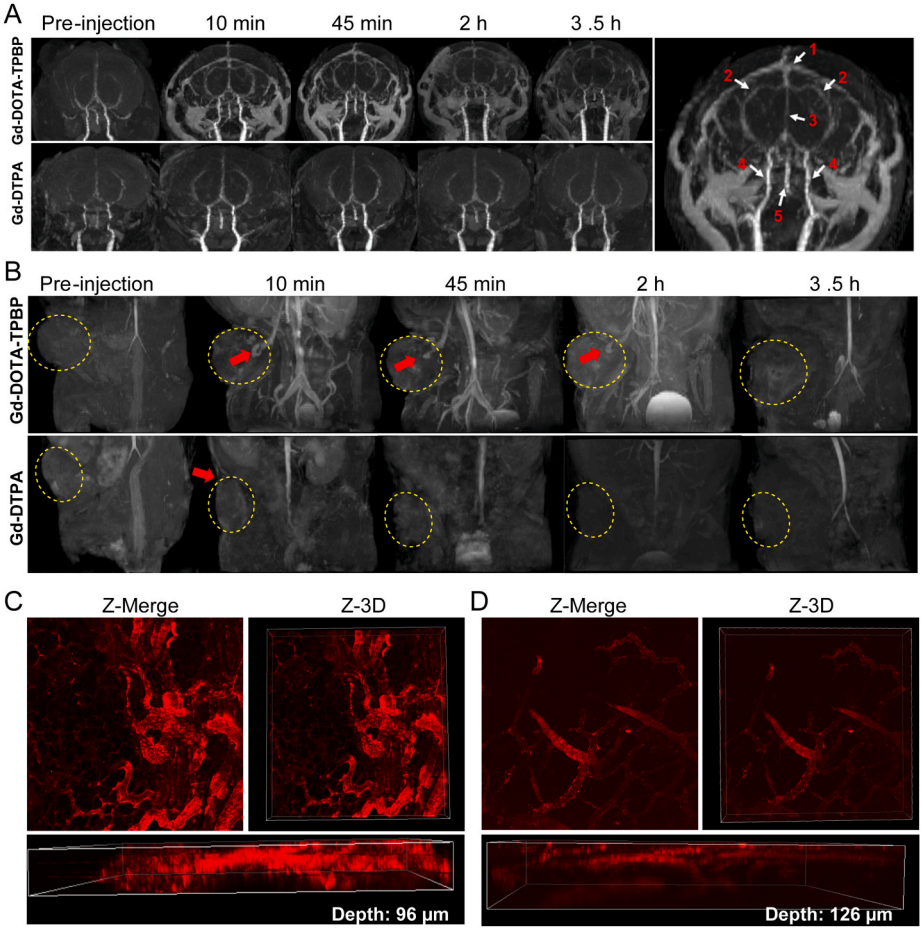

Fig. 3. Vascular images after injection of Gd-DOTA-TPBP. (A) Cerebrovascular enhanced MR images at different time points post injection of Gd-DOTA-TPBP or Gd-DTPA (n = 3). White arrows point to cerebral blood vessels. 1. superior sagittal sinus vein; 2. middle cerebral artery; 3. anterior cerebral artery; 4. internal carotid artery; 5. basilar artery. (B) Enhanced MRI scans of peritumor blood vessels at different time points post injection of Gd-DOTA-TPBP or Gd-DTPA. Red arrows point to the enhanced blood supply vessel of the tumor (n = 3). (C) Two-photon excitation confocal images of mouse brain blood vessels at 90 min post injection of Gd-DOTA-TPBP (n = 3). (D) Two-photon excitation confocal images of mouse tumor blood vessels at 90 min post injection of Gd-DOTA-TPBP (n = 3).

angiography has been rarely studied. Because of its less optical damage and deeper penetration depth in comparison with conventional single-photon excitation imaging, two-photon excitation (TPE) confocal microscopy imaging is more attractive for *in vivo* imaging. In this study, the blood vessels of the mouse brain and the tumor were scanned under a confocal laser scanning microscope (CLSM) in the two-photon mode after injection of Gd-DOTA-TPBP. A scanning depth of 126 μm was achieved via the TPE mode. At 90 min after Gd-DOTA-TPBP injection, blood vessels in the brain (Fig. 3C) and the tumor (Fig. 3D) were visible under the TPE CLSM and fluorescence signals were distinct in these blood vessels.

Because of high permeability of the tumor blood vessels, we also performed confocal TPE scanning of the tumor tissue at 24 h after injection of the contrast agent. Only blood vessels were observed in the tumor image at 90 min post injection (Fig. 3D), while the tissue surrounding these vessels was not seen, which indicated that Gd-DOTA-TPBP did not enter the tumor tissue from the tumor vasculature after blood circulation *in vivo* for 90 min. However, pronounced fluorescence signal in the tumor cells was detected at 24 h post injection (Fig. S15), indicated that Gd-DOTA-TPBP spread from the tumor vessels into the tumor tissue and was internalized by the tumor cells after 24 h blood circulation. Encapsulation of TPBP in micelles not only improved its water solubility, but also extended its clearance time by the kidney and reduced its toxicity, thus, Gd-DOTA-TPBP could be a great candidate for TPE CLSM FI.

MR angiography provided a comprehensive display of large vessels in the brain and the peritumor in mice, but failed to capture micro vessels. In contrast, although the imaging field was narrow, TPE CLSM FI could clearly reveal small blood vessels and even capillaries, and these FI images allowed tracking the penetration process of the contrast agent from tumor blood vessels into the tumor tissue and its cellular uptake process by tumor cells. Therefore, the combination of MR angiography and TPE CLSM FI successfully provided complementary information at both macroscopic and microscopic levels during vascular imaging of mice *in vivo*.

3.7. Contrast-enhancement imaging of the tumor

To evaluate the applicability of Gd-DOTA-TPBP as a contrast agent for tumor imaging, we used a clinical 3.0 T MRI scanner to detect MRI signals in a tumor-bearing mouse at different time points after injection of the contrast agent, and Gd-DTPA was set as a control (n = 3 for each group). In the Gd-DOTA-TPBP-treated group, the tumor exhibited enhanced signal at 10 min after injection of the contrast agent, and the enhanced signal appeared at the edge of the tumor. With an increase in the post injection time, the tumor enhancement became distinct and the signal enhancement region gradually shifted from the edge to the central part of the tumor (Fig. 4A). Semi-quantitative analysis of the tumor MRI signal showed that this enhancement continued to increase over time up to 2.5 h after injection of the contrast agent and then slowly decreased. At 8 h post injection of the contrast agent, the tumor signal intensity was still about 120% of that before the enhancement (Fig. 4B). In the Gd-DTPA-treated group (Fig. 4A), enhanced signal in the tumor was also found at 10 min after injection of the contrast agent, but the enhancement signal was homogeneously distributed in the entire tumor tissue. Pronounced enhancement in the signal in the tumor appeared at 45 min and 1.5 h after injection, but the signal became weak at time points after 1.5 h. Semi-quantitative analysis of the tumor signal revealed (Fig. 4B) that signal enhancement in the tumor peaked at 10 min post injection of Gd-DTPA and then slowly decreased. The signal values in the tumor at 4 h–8 h post injection had no significant difference in comparison with that at pre-injection. In addition, the relative enhancement of the peak signal in the tumor of the Gd-DOTA-TPBP group (171%) was higher than that in the Gd-DTPA group (135%) and the peak in the Gd-DOTA-TPBP group appeared at 2.5 h in comparison with 10 min in the Gd-DTPA group. These results may be due to two factors. First, Gd-DOTA-TPBP had a larger molecular weight, which may be associated with a longer circulation time *in vivo* so that it could accumulate in the tumor site through the EPR effect and the signal in the tumor could be intensified over a longer period of time. In contrast, Gd-DTPA was a small molecular contrast agent and it had a short circulation time *in vivo*, suggesting it could enter the tumor site quickly through tumor blood vessels. However, the retention time of Gd-DTPA was much shorter in the tumor site, and the enhanced tumor signal could retain for a short duration. Second,

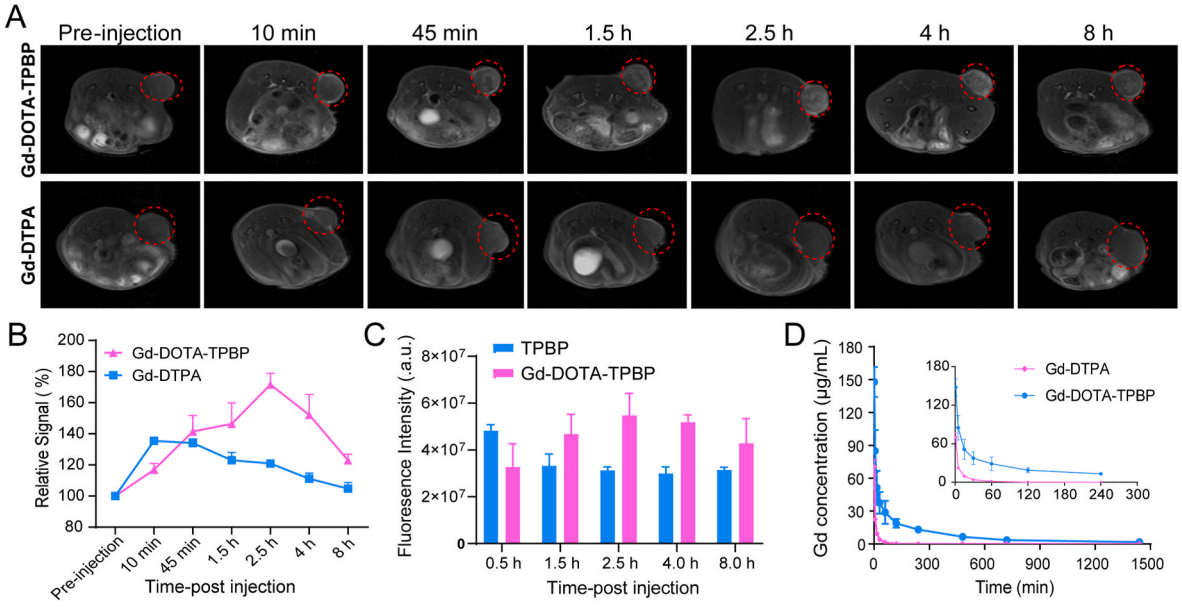

Fig. 4. Enhanced MRI/FI scans of the mouse tumor after injection of Gd-DOTA-TPBP and its pharmacokinetics. (A) *In vivo* MRI scan images of tumors after injection of Gd-DOTA-TPBP. The red dotted circles refer to the tumors. (B) Semi-quantitative analysis of relative MRI signal enhancement (n = 3). (C) Semi-quantitative analysis of fluorescence signal intensity in tumors after injection of Gd-DOTA-TPBP or TPBP (n = 3). (D) Pharmacokinetics of Gd-DOTA-TPBP and Gd-DTPA (n = 3).

a larger molecular weight of Gd-DOTA-TPBP endowed the contrast agent with a longer spin time in the solution, a higher aqueous phase relaxation rate, and a higher signal value than Gd-DTPA at the same gadolinium concentration. The results demonstrated that Gd-DOTA-TPBP could be used for tumor imaging in a prolonged manner with strong tumor enhancement signal at the same gadolinium dose compared with the clinical small molecule contrast agent Gd-DTPA, which could better distinguish the tumor from surrounding normal tissues.

To evaluate Gd-DOTA-TPBP as a fluorescent probe, we sacrificed tumor-bearing mice after Gd-DOTA-TPBP or TPBP injection, and detected fluorescence signal of the tumor *ex vivo* (n = 3 for each group). In TPBP treated group, the highest fluorescence signal in the tumor appeared at 0.5 h post injection (Fig. 4C), then decreased obviously with time. Semi-quantitative analysis showed fluorescence intensity decreased more than 30% from 0.5 h to 1.5 h post injection. In Gd-DOTA-TPBP treated group, fluorescence signal in the tumor at 0.5 h post injection was lower than that in TPBP treated group (Fig. 4C). And fluorescence signal had increased at later time point. Semi-quantitative analysis showed the fluorescence signal in the tumor in Gd-DOTA-TPBP treated group rose with time, reached the peak at 2.5 h, and then decreased slowly. At 8 h post injection, the fluorescence signal in Gd-DOTA-TPBP treated tumor was stronger than that in TPBP treated tumor. The trend of fluorescence signal in the tumor of two groups were similar with the trend of MRI signal, which indicated that Gd-DOTA-TPBP could be used as fluorescent probe and could acquired longer contrast-enhanced imaging time in tumor when compared with small molecule fluorescent probe.

We detected fluorescence signal of the main organs *ex vivo* as well. Fig. S16A and Fig. S16C showed in TPBP treated group, the fluorescence signal in liver was the highest at 0.5 h post injection, and then decreased obviously. The fluorescence signal in kidney was high at 0.5 h, and it kept relatively stable until 2.5 h, then it decreased. At 1.5 h and 2.5 h, fluorescence signals in kidney were higher than that in liver. This result indicated small molecule TPBP was excreted through liver and kidney, and kidney played a more important role at later period after injection. In Gd-DOTA-TPBP treated group (Fig. S16B and Fig. S16D), however, the highest fluorescence signal was in liver, which indicated that Gd-DOTA-TPBP was excreted from the model mainly through liver.

3.8. Pharmacokinetics of Gd-DOTA-TPBP

To assess the blood circulation time of Gd-DOTA-TPBP *in vivo*, ICP-MS was used for quantitative analysis of the gadolinium content in the blood at different time points post injection of the contrast agent. Because gadolinium was covalently linked to the polymeric backbone, the pharmacokinetics of gadolinium could be used for MRI and FI agents in the same nanocarrier. The blood gadolinium content in the Gd-DTPA group (Fig. 4D) decreased fast and its blood half-life was estimated to be 20.1 min (Table S2). A low molecular weight and a small size of Gd-DTPA led to rapid renal clearance and a short blood half-life. Although the gadolinium content in the Gd-DOTA-TPBP group temporally decreased, the decreasing rate was significantly slower compared with that in the Gd-DTPA group. Meanwhile, its blood half-life was estimated to be 468.5 min (Table S2), which was remarkably longer than that in the Gd-DTPA group. Since Gd-DOTA-TPBP had a high molecular weight and its hydrodynamic size was more than 20 nm, it was hardly subjected to renal elimination, thus, it had a longer blood circulation time than Gd-DTPA.

3.9. Contrast-enhanced MRI of main organs

A clinical 3.0 T MRI scanner was used to investigate the biodistribution of contrast agents by detecting MRI signal in the mouse main organs (liver, kidney and bladder) after injection of the contrast agent. The relative intensity of the peak signal in the bladder was the highest among three organs (Fig. 5A). The signal intensity in the bladder of the Gd-DTPA-treated group rose rapidly and the peak (444%, Fig. 5D) appeared at 45 min post injection, while the signal intensity decreased sharply after the peak time. This result was aligned with our assumption that Gd-DTPA could be excreted rapidly into the bladder via the kidney due to its small molecular weight and a short blood circulation time. However, it took a much longer time for Gd-DOTA-TPBP, a contrast agent with a high molecular weight, to be excreted through the kidney and then entered the bladder. Therefore, the signal intensity in the bladder had a slow gradient change in both increasing and decreasing periods (peak value 498%, Fig. 5D). Contrast-enhanced MR scans of the kidney (Fig. 5B) displayed that the signal intensity in the kidney of both Gd-DOTA-TPBP and Gd-DTPA groups increased significantly at 10 min after injection of contrast agents. The signal intensity in the Gd-DTPA group peaked at 10 min (134%, Fig. 5E), and then rapidly decreased. After 45 min, the signal intensity approached the same level as that before injection. Although the signal intensity in the kidney of the Gd-DOTA-TPBP group peaked at 10 min, its peak value was 194%, which was significantly higher than that in the Gd-DTPA group. In addition, the signal intensity in the kidney in the Gd-DOTA-TPBP group decreased in a much slower rate after 10 min post injection in comparison with the Gd-DTPA group. The signal in the kidney of the Gd-DOTA-TPBP group was still detectable until 8 h after injection. The MRI signal changes in the kidney were closely correlated with the MRI contrast-enhancement scanning results in the bladder. Fig. 5C showed that the MRI signal enhancement in the liver was not evident after injection of Gd-DTPA because it barely retained in the liver due to its small molecular weight. In contrast, significant MRI signal enhancement in the liver was found in the Gd-DOTA-TPBP group after injection of the contrast agent (186%, Fig. 5F) and the signal remained enhanced until 8 h post injection. Compared with small molecules, Gd-DOTA-TPBP as a macromolecule had a longer circulation time, so it could be readily phagocytosed by macrophages and then transported to the macrophage system of the liver [38], resulting in its aggregation in the liver and improved the contrast for MRI of the liver.

Because the MRI signal intensity is influenced by the relaxivity of contrast agents and fluorescence imaging signal intensity by the aggregation state of fluorophores, the results of MR and fluorescence imaging can not precisely reveal the biodistribution of Gd-DOTA-TPBP in the mouse. We applied ICP-MS to analyze the gadolinium content in the tumor and main organs after Gd-DOTA-TPBP injection to obtain quantitative biodistribution results. Gd-DTPA was used as a control. The time point of 2.5 h was chosen to investigate the biodistribution of Gd(III) since the signal in the tumor reached its peak in both MR and fluorescence images. Fig. S17A showed Gd(III) was mainly biodistributed in the liver in Gd-DOTA-TPBP treated group, and it could detect relative high content of Gd(III) in tumor as well. In Gd-DTPA treated group, Gd(III) was mainly biodistributed in the kidney. In total, the Gd(III) contents in Gd-DOTA-TPBP treated group were much higher than that in Gd-DTPA treated group. These results were consistent with the imaging data, and the high molecular weight, long circulation time of Gd-DOTA-TPBP could explain the results.

4. Conclusions

In this study, we successfully constructed an amphiphilic block polymer-based contrast agent, Gd-DOTA-TPBP, for dual-modality MR/fluorescence imaging. Gd-DOTA-TPBP could self-assemble into micelles in an aqueous solution and displayed the aggregation-induced emission effect for enhancing the fluorescence signal, thus, the fluorescence intensity of TPBP increased significantly after the formation of micelles. A higher r_1 value of Gd-DOTA-TPBP resulted in stronger signal intensity and sharper contrast enhancement in comparison with Gd-DTPA at the same gadolinium concentration. A large particle size and a high molecular weight of Gd-DOTA-TPBP prolonged its blood circulation time, and it performed better in vascular imaging than Gd-DTPA. A high level

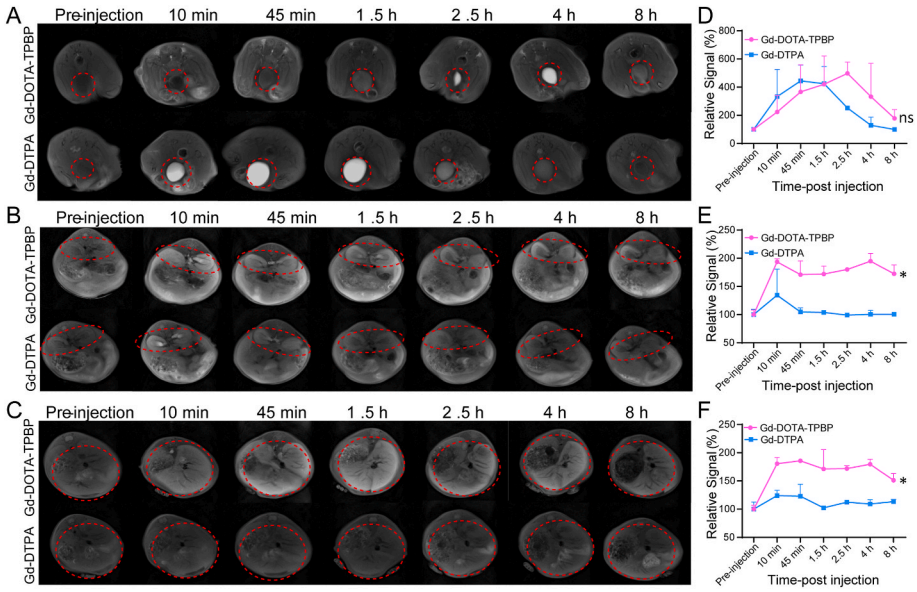

Fig. 5. Enhanced MR images of main organs of mice (n = 3). (A) MR images of the bladder. (B) MR images of the kidney. (C) MR images of the liver. (D) Semi-quantitative analysis of relative signal enhancement in the bladder. (E) Semi-quantitative analysis of relative signal enhancement in the kidney. (F) Semi-quantitative analysis of relative signal enhancement in the liver. The red dashed circles in (A–C) indicate the corresponding organs. *$p < 0.05$ for Gd-DOTA-TPBP vs Gd-DTPA.

of accumulation of Gd-DOTA-TPBP in tumors through the EPR effect combined with its higher r_1 value endowed the contrast agent with longer and better contrast enhancement than Gd-DTPA in MRI scans of the tumor. The characteristic of this contrast agent excited by two-photons allowed obtaining high-resolution confocal fluorescence *in vivo* images, which provided a successful example of complementary application of MRI and FI in contrast-enhanced angiography, and high sensitivity of the contrast agent for fluorescence imaging helped *in vivo* tracking of the agent over a long time. These results demonstrated that this amphiphilic block polymer-based contrast agent for dual-modality imaging could significantly improve the imaging performance of small molecule magnetic resonance contrast agents and fluorescent agents and the images from this contrast agent could provide complementary information at the cellular and tissue levels. It also had excellent biosafety. Therefore, it could be a great candidate of multimodal imaging contrast agents for biomedical applications.

CRediT authorship contribution statement

Xueyang Xiao: Conceptualization, Methodology, Investigation, Formal analysis, Data curation, Writing – original draft. **Hao Cai:** Methodology, Investigation, Formal analysis, Data curation, Funding acquisition, Writing – original draft. **Qiaorong Huang:** Methodology, Validation, Data curation, Software. **Bing Wang:** Methodology, Formal analysis, Validation, Funding acquisition. **Xiaoming Wang:** Methodology, Data curation. **Qiang Luo:** Methodology, Data curation. **Yinggang Li:** Data curation, Software. **Hu Zhang:** Writing – review & editing. **Qiyong Gong:** Supervision, Project administration. **Xuelei Ma:** Supervision, Resources, language and modification. **Zhongwei Gu:** Supervision, Project administration. **Kui Luo:** Supervision, Funding acquisition, Project administration, Resources, Writing – review & editing.

Declaration of competing interest

The authors declare that they have no known competing financial interests or personal relationships that could have appeared to influence the work reported in this paper.

Acknowledgments

This work was financially supported by National Natural Science Foundation of China (52073193, 51873120, 81621003 and 51903173), 1·3·5 Project for Disciplines of Excellence, West China Hospital, Sichuan University (ZYJC21013), Science and Technology Program of Sichuan province (2020YJ0231) and China Postdoctoral Science Foundation (2021M692255). The authors thank Sisi Wu, Zhiiqan Li, Yu Ding, Xuemei Chen, Li Fu, Huaiqiang Sun, Shenglan You, Lei Wu,Yaping Wu, Zheng Yang and Qing Yang (Research Core Facility, West China Hospital, Sichuan University) for their help in cell studies and histological studies.

Appendix A. Supplementary data

Supplementary data to this article can be found online at https://doi.org/10.1016/j.bioactmat.2022.04.026.

References

[1] D.E. Lee, H. Koo, I.C. Sun, J.H. Ryu, K. Kim, I.C. Kwon, Multifunctional nanoparticles for multimodal imaging and theragnosis, Chem. Soc. Rev. 41 (7) (2012) 2656–2672.
[2] H. Wang, B. Zhang, Y. Zhao, X. Chen, Z. Zhang, H. Song, Integrated effects of near-Field enhancement-induced excitation and surface plasmon-coupled emission of elongated gold nanocrystals on fluorescence enhancement and the applications in PLEDs, ACS Appl. Electron. Mater. 1 (10) (2019) 2116–2123.
[3] Z. Zhou, R. Bai, J. Munasinghe, Z. Shen, L. Nie, X. Chen, T1-T2 dual-modal magnetic resonance imaging: from molecular basis to contrast agents, ACS Nano 11 (6) (2017) 5227–5232.
[4] D.T. Wymer, K.P. Patel, W.F. Burke 3rd, V.K. Bhatia, Phase-contrast MRI: physics, techniques, and clinical applications, Radiographics 40 (1) (2020) 122–140.
[5] Z. Hu, C. Fang, B. Li, Z. Zhang, C. Cao, M. Cai, S. Su, X. Sun, X. Shi, C. Li, T. Zhou, Y. Zhang, C. Chi, P. He, X. Xia, Y. Chen, S.S. Gambhir, Z. Cheng, J. Tian, First-in-human liver-tumour surgery guided by multispectral fluorescence imaging in the visible and near-infrared-I/II windows, Nat. Biomed. Eng. 4 (3) (2020) 259–271.
[6] S. Wang, W.X. Ren, J.T. Hou, M. Won, J. An, X. Chen, J. Shu, J.S. Kim, Fluorescence imaging of pathophysiological microenvironments, Chem. Soc. Rev. 50 (16) (2021) 8887–8902.
[7] S. Guo, X. Xiao, X. Wang, Q. Luo, H. Zhu, H. Zhang, H. Li, Q. Gong, K. Luo, Reductive microenvironment responsive gadolinium-based polymers as potential safe MRI contrast agents, Biomater. Sci. 7 (5) (2019) 1919–1932.
[8] J.V. Jun, D.M. Chenoweth, E.J. Petersson, Rational design of small molecule fluorescent probes for biological applications, Org. Biomol. Chem. 18 (30) (2020) 5747–5763.
[9] A. Berdichevski, H. Simaan Yameen, H. Dafni, M. Neeman, D. Seliktar, Using bimodal MRI/fluorescence imaging to identify host angiogenic response to implants, Proc. Natl. Acad. Sci. U.S.A. 112 (16) (2015) 5147–5152.
[10] K. Li, D. Ding, D. Huo, K.-Y. Pu, N.N.P. Thao, Y. Hu, Z. Li, B. Liu, Conjugated polymer based nanoparticles as dual-modal probes for targeted in vivo fluorescence and magnetic resonance imaging, Adv. Funct. Mater. 22 (15) (2012) 3107–3115.
[11] F. Su, S. Agarwal, T. Pan, Y. Qiao, L. Zhang, Z. Shi, X. Kong, K. Day, M. Chen, D. Meldrum, V.D. Kodibagkar, Y. Tian, Multifunctional PHPMA-derived polymer

for ratiometric pH sensing, fluorescence imaging, and magnetic resonance imaging, ACS Appl. Mater. Interfaces 10 (2) (2018) 1556–1565.
[12] K.J. Thurecht, Polymers as probes for multimodal imaging with MRI, Macromol. Chem. Phys. 213 (24) (2012) 2567–2572.
[13] A.W. York, S.E. Kirkland, C.L. McCormick, Advances in the synthesis of amphiphilic block copolymers via RAFT polymerization: stimuli-responsive drug and gene delivery, Adv. Drug Deliv. Rev. 60 (9) (2008) 1018–1036.
[14] L. Luo, Y. Qi, H. Zhong, S. Jiang, H. Zhang, H. Cai, Y. Wu, Z. Gu, Q. Gong, K. Luo, GSH-sensitive polymeric prodrug: synthesis and loading with photosensitizers as nanoscale chemo-photodynamic anti-cancer nanomedicine, Acta Pharm. Sin. B 12 (1) (2022) 424–436.
[15] D. Huang, Y. Liu, A. Qin, B.Z. Tang, Recent advances in alkyne-based click polymerizations, Polym. Chem. 9 (21) (2018) 2853–2867.
[16] H. Wang, Y. Bo, Y. Liu, M. Xu, K. Cai, R. Wang, J. Cheng, In vivo cancer targeting via glycopolyester nanoparticle mediated metabolic cell labeling followed by click reaction, Biomaterials 218 (2019), 119305.
[17] X. Zheng, D. Pan, X. Chen, L. Wu, M. Chen, W. Wang, H. Zhang, Q. Gong, Z. Gu, K. Luo, Self-stabilized supramolecular assemblies constructed from PEGylated dendritic peptide conjugate for augmenting tumor retention and therapy, Adv. Sci. 8 (22) (2021), e2102741.
[18] P. Caravan, J.J. Ellison, T.J. McMurry, R.B. Lauffer, Gadolinium(III) chelates as MRI contrast agents: structure, dynamics, and applications, Chem. Rev. 99 (9) (1999) 2293–2352.
[19] S. Subasinghe, J. Romero, C.L. Ward, M.D. Bailey, D.R. Zehner, P.J. Mehta, F. Carniato, M. Botta, J.T. Yustein, R.G. Pautler, M.J. Allen, Magnetic resonance thermometry using a Gd(III)-based contrast agent, Chem. Commun. 57 (14) (2021) 1770–1773.
[20] C. Guo, L. Sun, W. She, N. Li, L. Jiang, K. Luo, Q. Gong, Z. Gu, A dendronized heparin–gadolinium polymer self-assembled into a nanoscale system as a potential magnetic resonance imaging contrast agent, Polym. Chem. 7 (14) (2016) 2531–2541.
[21] X. Hu, G. Liu, Y. Li, X. Wang, S. Liu, Cell-penetrating hyperbranched polyprodrug amphiphiles for synergistic reductive milieu-triggered drug release and enhanced magnetic resonance signals, J. Am. Chem. Soc. 137 (1) (2015) 362–368.
[22] Y. Huang, J. Xing, Q. Gong, L.C. Chen, G. Liu, C. Yao, Z. Wang, H.L. Zhang, Z. Chen, Q. Zhang, Reducing aggregation caused quenching effect through co-assembly of PAH chromophores and molecular barriers, Nat. Commun. 10 (1) (2019) 169.
[23] H. Gao, C. Kam, T.Y. Chou, M.Y. Wu, X. Zhao, S. Chen, A simple yet effective AIE-based fluorescent nano-thermometer for temperature mapping in living cells using fluorescence lifetime imaging microscopy, Nanoscale Horiz 5 (3) (2020) 488–494.
[24] Q. Chen, C. Jia, Y. Zhang, W. Du, Y. Wang, Y. Huang, Q. Yang, Q. Zhang, A novel fluorophore based on the coupling of AIE and ESIPT mechanisms and its application in biothiol imaging, J. Mater. Chem. B 5 (37) (2017) 7736–7742.
[25] Q. Lu, C. Yang, X. Qiao, X. Zhang, W. Cai, Y. Chen, Y. Wang, W. Zhang, X. Lin, H. Niu, W. Wang, Multifunctional AIE-active polymers containing TPA-TPE moiety for electrochromic, electrofluorochromic and photodetector, Dyes Pigments 166 (2019) 340–349.
[26] H. Nie, B. Chen, J. Zeng, Y. Xiong, Z. Zhao, B.Z. Tang, Excellent n-type light emitters based on AIE-active silole derivatives for efficient simplified organic light-emitting diodes, J. Mater. Chem. C 6 (14) (2018) 3690–3698.
[27] L. Zhou, X. Zhang, Q. Wang, Y. Lv, G. Mao, A. Luo, Y. Wu, Y. Wu, J. Zhang, W. Tan, Molecular engineering of a TBET-based two-photon fluorescent probe for ratiometric imaging of living cells and tissues, J. Am. Chem. Soc. 136 (28) (2014) 9838–9841.
[28] B. Ma, W. Zhuang, H. He, X. Su, T. Yu, J. Hu, L. Yang, G. Li, Y. Wang, Two-photon AIE probe conjugated theranostic nanoparticles for tumor bioimaging and pH-sensitive drug delivery, Nano Res. 12 (7) (2019) 1703–1712.
[29] R. Zhang, J. Yang, M. Sima, Y. Zhou, J. Kopecek, Sequential combination therapy of ovarian cancer with degradable N-(2-hydroxypropyl)methacrylamide copolymer paclitaxel and gemcitabine conjugates, Proc. Natl. Acad. Sci. U.S.A. 111 (33) (2014) 12181–12186.
[30] L. Sun, X. Li, X. Wei, Q. Luo, P. Guan, M. Wu, H. Zhu, K. Luo, Q. Gong, Stimuli-responsive biodegradable hyperbranched polymer-gadolinium conjugates as efficient and biocompatible nanoscale magnetic resonance imaging contrast agents, ACS Appl. Mater. Interfaces 8 (16) (2016) 10499–10512.
[31] B. Wang, H. Li, Z. Li, Q. Luo, Z. Gu, H. Zhang, Q. Gong, K. Luo, Amphiphilic block polymer-gadolinium conjugates: design, synthesis and application as efficient and safe nanoscale magnetic resonance imaging contrast agents, Chem. Eng. J. 416 (2021), 129170.
[32] J. Zhang, H. Song, S. Ji, X. Wang, P. Huang, C. Zhang, W. Wang, D. Kong, NO prodrug-conjugated, self-assembled, pH-responsive and galactose receptor targeted nanoparticles for co-delivery of nitric oxide and doxorubicin, Nanoscale 10 (9) (2018) 4179–4188.
[33] Y. Li, T.Y. Lin, Y. Luo, Q. Liu, W. Xiao, W. Guo, D. Lac, H. Zhang, C. Feng, S. Wachsmann-Hogiu, J.H. Walton, S.R. Cherry, D.J. Rowland, D. Kukis, C. Pan, K. S. Lam, A smart and versatile theranostic nanomedicine platform based on nanoporphyrin, Nat. Commun. 5 (2014) 4712.
[34] X. Zhang, K. Wang, M. Liu, X. Zhang, L. Tao, Y. Chen, Y. Wei, Polymeric AIE-based nanoprobes for biomedical applications: recent advances and perspectives, Nanoscale 7 (27) (2015) 11486–11508.
[35] L. Wang, M. Huang, H. Tang, D. Cao, Y. Zhao, Fabrication and application of dual-modality polymer nanoparticles based on an aggregation-induced emission-active fluorescent molecule and magnetic Fe_3O_4, Polymers 11 (2) (2019) 220.
[36] L. Zhang, H. Xue, Z. Cao, A. Keefe, J. Wang, S. Jiang, Multifunctional and degradable zwitterionic nanogels for targeted delivery, enhanced MR imaging, reduction-sensitive drug release, and renal clearance, Biomaterials 32 (20) (2011) 4604–4608.
[37] A. Gruneboom, L. Kling, S. Christiansen, L. Mill, A. Maier, K. Engelke, H.H. Quick, G. Schett, M. Gunzer, Next-generation imaging of the skeletal system and its blood supply, Nat. Rev. Rheumatol. 15 (9) (2019) 533–549.
[38] S.Y. Fam, C.F. Chee, C.Y. Yong, K.L. Ho, A.R. Mariatulqabtiah, W.S. Tan, Stealth coating of nanoparticles in drug-delivery systems, Nanomaterials 10 (4) (2020) 787.